

Changes in the African monsoon region at medium-term time horizon using 12 AR4 coupled models under the A1b emissions scenario.

Bernard Fontaine, Pascal Roucou, Paul-Arthur Monerie

Centre de Recherches de Climatologie, UMR5210, CNRS / University of Burgundy, Dijon, France

(33) 03 80 39 57 43

(33) 03 80 39 57 41

fontaine@u-bourgogne.fr

<http://climatologie.u-bourgogne.fr/>

Abstract.

This study documents simulated precipitation and circulation changes through the 20C3M and A1b scenario. The portray a robust pattern, associating rainfall deficits in subtropical regions with excesses over West Africa, except in Northern Senegal and Mauritania, with a significant enhancement of both the April-June rainy season in 10/12 models and of the July-September rainy season in 8/12 models. Eastward to 5°W a northward shift in latitude of the moisture flux convergence at 850 hPa is evident in 10/11 models (+0.58 ° in mean) and a southward shift in 6 /11 models in the western region (-0.24°) is observed.

African monsoon, Climate change, Precipitation, West Africa

1. Introduction

Some authors asserted that the partial recovery of Sahel precipitation since the 1990s could be a response to greenhouse gas forcing through an increased temperature contrast between land and ocean, since a wetter Sahel might follow from an enhanced warming of land compared to oceans, which would be responsible for driving a stronger monsoonal flow inland (Paethe and Hense, 2004). For Hoerling et al. (2006), Maynard et al. (2002) and Haarsma et al. (2005) a future wetter Sahel can be conceived as the response to a reversal in sea surface temperature pattern in the Atlantic Ocean due either to a reduction of aerosol loading, or to the Atlantic multi-decadal oscillation. However it could be premature to take this partial rainfall amelioration as evidence of a global warming signature, given the likely influence of internal variability on the inter-hemispheric SST gradients that influence Sahel rainfall, as well as the influence of

aerosol variations (Christensen et al., 2007) and the flawed representations of the WAM climate (Cook and Vizu, 2006). However, recently, Giannini (2010) has pointed out that the increase in anthropogenic greenhouse gases drives a direct continental change in the Sahel region: the increase in net terrestrial radiation at the surface is amplified by the water vapor feedback which increases evaporation, favouring vertical instability and near-surface convergence.

Some AR4 20C3M simulations (20th century runs using historical GHG concentrations, 1871-2000), can produce unrealistic variability in the Sahel with systematic errors and large model differences (Christensen et al., 2007; Paethe et al., 2008). This is partly due to the different parameterizations of clouds and convection, to the omission of dynamic vegetation (Giannini et al., 2003) and to the quasi-absence of feedbacks from dust aerosol production and from future land surface modification in projections.

The goal of this paper is to identify precipitation changes and associated atmospheric signals in North Africa at medium-term time horizon through a multi-model (MM) ensemble approach based on the 20C3M simulations and A1b emissions scenario from 12 ocean-atmosphere coupled models. We will focus on the April-June and July-September rainy seasons observed in the Guinean and Sudan-Sahel, respectively. These choices are hence different from most studies conducted to date including the last IPCC report which concentrated more on the June-August climate changes between years 1980-1999 and 2080-2099, and concluded on non-robust response with modest moistening in the Sahel with little change on the Guinean coast (Christensen et al., 2007). The choice of a relatively short time horizon (50 years) may also increase the generality of the results since before 2050, CO₂ emissions and concentrations in A1b are very similar to those projected by scenarios from the A2 family.

2. Data and Methods

The A1b scenario provides a good mid-line scenario for CO₂ emission and economic growth and supposes a balanced emphasis on all energy sources. The MM approach is based on 12 runs issued from 12 different coupled models (see table 1 more details on <http://www.ipcc.ch>): Joly and Voltaire (2009) have

shown that this set offers a representative sample of the performance of state-of-the-art coupled models without any type of a priori consideration.

Precipitation change and associated signals are estimated by comparing the seasonal rainfall outputs simulated by the 12 models, between years 1960-1999, the 'current period', and 2031-2070, the 'near future', using in cooperation (i) the MM approach, (ii) the 'one model one vote' concept (Santer et al., 2009) and (iii) individual differences taken with respect to each model climatology. The 'current period' includes a comprehensive set of both abnormally wet years (in the 60s and 90s) and abnormally dry years (within the 70s and 80s).

The CRU TS 2.1 at 0.5° resolution (Mitchell et al., 2002) and the GPCP at 2.5° (Adler et al., 2003) datasets will be used as observational reference for estimating the continental rainfall.

The simulated changes will be presented as seasonal means and composite fields and through (i) rainfall indexes depicting the April-June Guinean rainy season and the July-September monsoon season, (ii) atmospheric indexes describing the mean location of moisture flux convergence at 850 hPa, and (iii) near-surface temperatures, moisture fluxes and meridional gradients of moist static energy over West Africa.

3. Rainfall patterns

The July-September ensemble-mean (figure 1a) shows first that models have difficulties in reproducing the observed northward penetration of the rain belt deep into the continent: this belt stands abnormally southward (7-8°N vs ~10°N in observation) due to an insufficient simulated upwelling off the West Coast -by 3°C off the southwest coast- (Christensen et al., 2007).

Nonetheless, the precipitation change (figure 1b), shows that the largest drying is simulated within the whole Mediterranean and Southern European domain in agreement with conclusions for the end of the 21st century (Christensen et al., 2007). However our results exhibits a significant composite pattern with increasing rainfall over the central and eastern Sahel regions and negative

differences in the Guinean Gulf and western Sahel: rainfall excesses are encountered by 12°N in the eastern Atlantic and central Sahel in association with rainfall deficits over the Gulf of Guinea. This supposes a deeper northward penetration of the rain belt associated with an enhancement of the monsoon circulation since GES scenarios produce stronger warming in northern tropical Atlantic, southern Europe and Mediterranean areas than in the moister tropics (Christensen et al., 2007). The generated SST anomaly pattern in the Atlantic and the Mediterranean is favorable to a more northward excursion of the monsoon (Garcia-Serrano et al., 2008; Fontaine et al., 2009) while the meridional surface temperature anomaly gradient over West Africa tends to shift farther north the African Easterly Jet which is also associated with a larger rainfall over Sahel (Hourdin et al., 2010).

Figure 1c displays the number of models simulating positive and negative JAS differences after giving to each model the same weight (see the caption). Rainfall deficits are observed in subtropical regions and rainfall excesses over a large WAM area, except in Northern Senegal and Mauritania. The largest positive scores (+8) are encountered over central Sahel by 12°N, just northward to the mean location of the rain-belt in the models (figure 1a); the largest negative scores (< -10) are located in the northern subtropics and south of the equator. Precipitation change in West Africa is, overall, positive and denotes a deeper penetration of the monsoon into the continent mainly eastward to 10°E. Conversely, the change is negative over areas of large-scale subtropical subsidence, especially in the Mediterranean and Eastern Atlantic regions. Interestingly precipitation changes simulated by the 12 individual models (not shown) indicate that most models simulate similar patterns to those displayed in figure 1b,c,d., in particular CNRM, NCAR, CCCMA, UKMO and MPI.

4. Regional rainfall and associated changes

Regional indexes have been first defined by averaging in each model the seasonal rainfall amounts on 2 specific key-regions: the April-June season in the Gulf of Guinea [Eq-5N; 20W-10E] and the July-September season over the Western and Eastern continental parts of West Africa (see table2). Most models are often close to the observed mean, except those listed at right, but tend to

underestimate the interannual standard deviations and coefficients of variation because the inter-annual variability of SST is very weak in the Gulf of Guinea (Joly and Voldoire 2010).

Mean annual evolutions (figure 2a-c) show that (i) only one half of the models reproduce a clear seasonal cycle while the mean model ensemble fails on this aspect; (ii) the models which perform at best on a region or season do not success necessarily on other regions and seasons, except for INMCM, IPSL and MRI which simulate the lowest seasonal cycles and rainfall amounts.

Composites in figure 2d-i display, for each model and month, the precipitation changes: a clear enhancement of April-July amounts is found over the equatorial Atlantic, with 10 boxes showing significant excesses in figure 2d (vs 2 deficits). On the whole, 10 models out of 12 produce an April-June increase of the median and quartile values (figure 2g). Changes in July-September are less obvious on the western part of Africa: no signal with the multi-ensemble mean (figure 2h) and only 6/3 models produce significant positive/negative differences (figure 2h). By contrast, over the eastern part (figure 2i), the multi-model ensemble and 9/12 models simulate higher rainfall.

Such modification in Sahelian rainfall increase and shift in latitude are associated with coherent changes in the West African monsoon circulation. For example, the moisture flux convergence at 850 hPa in boreal summer is also shifted northward (southward) (figure 2j,k): eastward (westward) to the zero longitude, this displacement is observed in 10/11 (6/11) individual models with a $+0.58^\circ$ (-0.24°) shift in the multi-model. These values are significant at $p=0.05$.

Changes in surface air temperature and moisture flux at 925 hPa are also very significant. Thus, figure 3b,e denotes a reinforced monsoon flux over West Africa and India, in association with continental warming over the northern tropical deserts and, in July-September, all around the Mediterranean. This thermal pattern tends to strengthen both the Saharan heat low (Fig.3d,e) and the meridional temperature gradients known to be linked to the horizontal moist static energy gradients driving the monsoon circulation (Fontaine et al., 1999). It is worth noting that all individual models and the multi-model mean produce such a temperature gradient enhancement during the two April-June and July-September rainy seasons over the Guinean and Sahelian regions (Fig.3c,f). Since the moisture and thermal gradients impact the AEJ location in regional climate model outputs

(Bamba Sylla et al., 2009), these changes could therefore impact the future African monsoon.

5. Conclusion

The goal of this study was to document the April-June and July-September precipitation changes in the African monsoon region by contrasting the 40-year periods 1960-1999 and 2031-2070. The results showed that model accuracy depends on the ability to reproduce the observed mean seasonal cycle. The simulated changes around the middle of this century are spatially coherent and locally significant. They reproduce a typical anomaly pattern contrasting rainfall deficits in the subtropical regions, and rainfall excesses over a large West African monsoon area, except in Northern Senegal and Mauritania.

Analyses of a few key-regional indices denoted also lower (higher) occurrence of anomalous dry (wet) rainy seasons. Rainfall increases are attested in 10 models out of 12 during the April-June rainy season in the Gulf of Guinea, and in 8 models out of 12 for the July-September amounts over the central and eastern Sahel. In July-September the rainfall pattern contrasts excesses around 12°N in the eastern Atlantic and central Sahel and deficits over the Gulf of Guinea. Moreover eastward to the zero longitude a northward shift in latitude of the moisture flux convergence at 850 hPa is evident in 10/11 models (+0.58 ° in mean) but a southward shift in 6/11 models in the western region (-0.24°) is observed. Associated changes in near-surface temperature, moisture fluxes and meridional temperature gradients are significant in near-all models and denote a more vigorous monsoon penetrating deeper into the West African continent. In a future paper we will focus on the atmospheric conditions associated with the global warming to explain the differential effect on the western and central-eastern Sahel, and therefore contribute to reduce uncertainty on the global warming effect in the region.

Acknowledgements:

The study was supported by the Global change and Ecosystems programme (EU Integrated project: African Monsoon Multidisciplinary Analysis (AMMA) and the French component of AMMA. Based on a French initiative, AMMA was built by an international scientific group and is

currently funded by a large number of agencies, especially from France, UK, US and Africa. The authors are very grateful to the modelling teams for providing outputs.

References

- Adler RF, GJ Huffman, A Chang, R Ferraro, P Xie, Janowiak J, Rudolf B, Schneider U, Curtis S, Bolvin D, Gruber A, Susskind J, Arkin P, Nelkin E, 2003. The version-2 global precipitation climatology project (GPCP) monthly precipitation analysis (1979-present), *J Hydrometeor* :, 1147-1167.
- Bamba Sylla M, Coppola E, Mariotti L, Giorgi F, Ruti PM, Dell'Aquila A, Bi X 2009. Multiyear simulation of the African climate using a regional climate model (RegCM3) with the high resolution ERA-interim reanalysis. *Climate Dynamics*, Online publication date: 2-Jul-2009.
- Christensen JH, B Hewitson, Busuioc A, Chen A, Gao X, Held I, Jones R, Kolli RK, Kwon WT, Laprise R, Magaña Rueda V, Mearns L, Menéndez CG, Räisänen J, Rinke A, Sarr A, Whetton P. 2007. Regional Climate Projections. In: *Climate Change 2007: The Physical Science Basis*. Cambridge University, Press, Cambridge.
- Cook KH, Vizzy EK. 2006. Coupled Model Simulations of the West African Monsoon System: 20th century Simulations and 21st Century Predictions. *J. Climate*, 19: 3681-3703.
- Fontaine B, Philippon N, Camberlin P. 1999. An improvement of June-September rainfall forecasting in the Sahel based upon region April-May moist static energy content (1968-1997). *Geophys. Res. Lett.*, 26: 2041-2044.
- Fontaine B, Garcia-Serrano J, Roucou P, Rodriguez-Fonseca B, Losada T, Chauvin F, Gervois S, Sivarajan S, Ruti P, Janicot S. 2009. Impacts of Warm and Cold situations in the Mediterranean Basins on the West African monsoon: observed connection patterns (1979-2006) and climate simulations. *Climate Dynamics*, ISSN0930-7575 (Print) 1432-0894 (Online), DOI 10.1007/s00382-009-0599-3.
- Garcia-Serrano J, Losada T, Rodriguez-Fonseca B, Polo I, 2008. Tropical Atlantic Variability Modes (1979-2002). Part II: Time-Evolving Atmospheric Circulation Related to SST-Forced Tropical Convection. *Journal of Climate*, 21 (24): 6476-6497.
- Giannini A, Saravanan R, Chang P. 2003. Oceanic forcing of Sahel rainfall on interannual to interdecadal time scales. *Science* 302, 1027–1030.
- Giannini A. 2010. Mechanisms of climate change in the semi-arid African Sahel. the local view, *Journal of. Climate* **23**: 743-756
- Haarsma RJ, Selten F, Weber N, Kliphuis M. 2005. Sahel rainfall variability and response to greenhouse warming, *Geophysical Research Letters* DOI [10.1029/2005GL023232](https://doi.org/10.1029/2005GL023232).
- Hoerling MP, Hurrell JW, Eischeid J. 2006. Detection and attribution of 20th century Northern and Southern African monsoon change. *Journal of Climate* 19(16): 3989–4008.
- Hourdin F, Musat I, Guichard F, Ruti PM, Favot F, Filiberti MA, Pham M, Grandpeix JY, Polcher J, Marquet P, Boone A, Lafore JP, Redelsperger JL, Dell'Aquila A, Losada Doval T, Khadre Traore A, Gallée H. 2010. AMMA-Model Intercomparison Project, *BAMS* DOI:10.1175/2009BAMS2791.1
- Joly M, A. Voltaire. 2009. Role of the Gulf of Guinea and the Mediterranean in the interannual variability of the West African monsoon. *Climate Dynamics* 10.1002/joc.2026.
- Joly M, Voltaire A. 2010. Role of the Gulf of Guinea in the inter-annual variability of the West African monsoon: what do we learn from CMIP3 coupled simulations? *International Journal of Climatology* 30, DOI - 0.1002/joc.2026: 1843- 1856.
- Maynard K, Royer JF, Chauvin F. 2002. Impact of greenhouse warming on the West African summer monsoon. *Climate. Dynamics* 19: 499–514.
- Mitchell TD, Hulme M, New M. 2002. Climate data for political areas. *Area* **34**: 109-112.
- Paeth H and Hense A. 2004. SST versus climate change signals in West African rainfall: 20th-century variations and future projections. *Climatic Change* 65(1–2): 179–208
- Randall DA, Wood RA, Bony S, Colman R, Fichet T, Fyfe J, Kattsov V, Pitman A, Shukla J, Srinivasan J, Stouffer RJ, Sumi A, Taylor KE. 2007. *Climate Models and Their Evaluation*. Climate Change 2007: The Physical Science Basis. Contribution of York, NY, USA.
- Santer B D, Taylor K E, Gleckler P J, Bonfils C, Barnett T P, Pierce DW, Wigley TML, Mears C, Wentz FJ, Braggemann W, Gillett N P, Klein SA, Solomon S, Stott PA, Wehner MF. 2009. Incorporating model quality information in climate change detection and attribution studies, *Proceedings of the National Academy of Sciences* 106, 35: 14778-14783.

Figure 1: Simulated rainfall in JAS as simulated by the 12 models listed in Table 1:

- (a) mean rainfall for the current period in mm/day;
- (b) precipitation change in mm/day between years 2031-2070 and 1960-1999; the superimposed asters refer to significant differences at $p=0.05$ using a Student t -test..
- (c) Number of models simulating a deficit (negative values) or an excess (positive values) by grid-points, i.e., the scores range either between +7 and +12 or between -7 and -12: +7 (-7) means that 7 models out of 12 simulate increasing (decreasing) rainfall and +12 (-12) that all models produce an excess (a deficit).

Figure 2: Simulated seasonal indexes averaged over key-regions,

(a,b,c) mean annual rainfall evolutions over the Gulf of Guinea [Eq-5N; 20W-10E] from April to June (1st column) and over the Western [5N-20N; 20W-0E] and Eastern [5N-20N; 0E-30E] continental parts of West Africa (columns 2-3). Model acronyms (y-axis) are sorted in descending order regarding individual seasonal amounts with the mean model ensemble at top

(d,e,f) significant ($p= 0.05$) precipitation change expressed in percents between years 1960-1999 and 2031-2070.

(g,h,i) notched-box plot as robust estimate of the uncertainty about the medians for box to box comparison. Each box has lines at the lower quartile, median, and upper quartile values, all expressed in percentages of precipitation change. Lines extending from each end of the box show the extent of the rest of the data between -50% and + 50%.

(j,k) as (g,h,i) but for the latitudinal location in degree of the centroid of the moisture flux convergence at 850 hPa averaged over a western (15°W -5°W; 0°-14°N) and a central-eastern (5°W- 20°E; 0°N-20°N) African regions. Here only 11 models out of 12 are considered since no moisture data were available in UKMO.

Figure 3. Simulated changes in air temperature near the surface, in moisture flux at 925 hPa (maps), and in air temperature gradients (boxplots) in AMJ (left) and JAS (right)
(a,d): temperature in tenth of °C and moisture fluxes in g/kg/m/s from the ensemble mean (1960-1999)
(b,e): differences in air temperature at 2m and in moisture fluxes at 925 hPa between years 1960 1999 and 2031-2070
(c,f): notched-box plot (as in fig. 2g-i), but for changes (in °C) in meridional air temperature gradient at 2m between 10°W and 0°longitude. In April-June (AMJ) the gradient refers to the difference between values averaged over [7.5°N-12.5°N] and over [5°S-Eq] while in July-September (JAS) the gradient is the difference between [20°N-15°N] and [5°S-Eq].

Tables

Models	Grids long x lat x lev	Models	Grids long x lat x lev
CCMA : Canadian Centre for Climate Modelling and Analysis, Canada	96 x 48 x 17	MIROC : Center for Climate System Research, + Institute for Environmental Studies, +Frontier Research Center for Global Change, Japan	128 x 64 x 17
GFDL : Geophysical Fluid Dynamics Laboratory, USA	144 x 90 x 17	NCAR : National Center for Atmospheric Research, USA	256 x 128x17
IPSL : Institut Pierre Simon Laplace, France	96 x 72 x 17	CSIRO : CSIRO Atmospheric Research, Melbourne, Australia	192x96x17
MRI Meteorological Research Institute, Japan	128 x 64 x 17	INMCM Institute for Numerical Mathematics, Russia	72x45x17
CNRM Centre National de Recherches Meteorologiques, France	128 x 64 x 17	MPI : Max Planck Institute for Meteorology, Germany	192x96x16
GISS Goddard Institute for Space Studies, New York, NY, USA	72 x 45 x 17	UKMO : Met Office UK	96 x 73 x 15 ;

Table 1: The 12 models and groups. More details in Randall et al. (2007), their table 8.1 (pp 597-598).

WAMW	<u>CRU</u>	<u>GPCP</u>	gfdl	miroc	ukmo	cccma	ncar	mpi	giss	csiro	inmcm	cnrm	mri	ipsl
Mean	<u>5.6</u>	<u>5.9</u>	8.6	7.1.	5.8*	5.6*	5.4*	5.4*	4.5	4.3	3.7	3.3	3.2	3.2
STD	<u>0.7</u>	<u>0.7</u>	0.8	0.7	0.6	0.5	0.3	0.5	0.7	0.4	0.4	0.5	0.4	0.3
CV %	<u>12.7</u>	<u>11.7</u>	9.2	9.8	10.0	8.4	5.3	9.5	14.9	8.6	11.5	13.8	10.8	8.5
WAME	<u>CRU</u>	<u>GPCP</u>	cnrm	miroc	gfdl	cccma	ncar	ukmo	csiro	mpi	mri	giss	inmcm	ipsl
Mean	<u>4.3</u>	<u>4.3</u>	5.6	5.6	4.8	4.5*	4.4*	4.2*	3.7	3.4	3.2	2.7	2.5	1.9
STD	<u>0.5</u>	<u>0.5</u>	0.5	0.6	0.7	0.4	0.2	0.5	0.3	0.3	0.2	0.4	0.3	0.1
CV %	<u>11.4</u>	<u>11.1</u>	9.6	11.5	13.8	8.2	4.6	12.5	8.4	10.3	6.2	13.8	11.6	7.2

Table 2: July-September rainfall means (in mm/day), interannual standard deviations (STD) and coefficients of variation (STD/mean) in observations (CRU, underlined) and individual simulations (period 1960-1999) averaged over the western (20W-0°) and Eastern (0°-30°E) parts of West Africa (5°N-20°N): WAMW and WAME, respectively. Model acronyms are arranged from left to right in descending order relatively to the mean. The simulated JAS means not significantly different from observations regarding a Student t-test at p=0.05 are bolded with an aster.

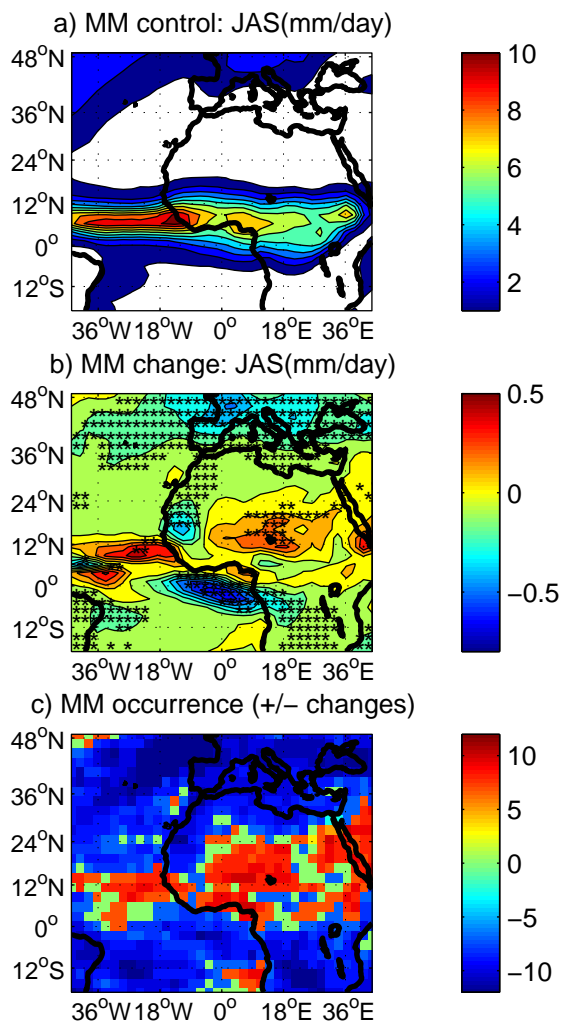


Figure 1: Simulated rainfall in JAS as simulated by the 12 models listed in Table 1:

(a) mean rainfall for the current period in mm/day;

(b) precipitation change in mm/day between years 2031-2070 and 1960-1999; the superimposed asters refer to significant differences at $p=0.05$ using a Student t -test..

(c) Number of models simulating a deficit (negative values) or an excess (positive values) by grid-points, i.e., the scores range either between +7 and +12 or between -7 and -12: +7 (-7) means that 7 models out of 12 simulate increasing (decreasing) rainfall and +12 (-12) that all models produce an excess (a deficit).

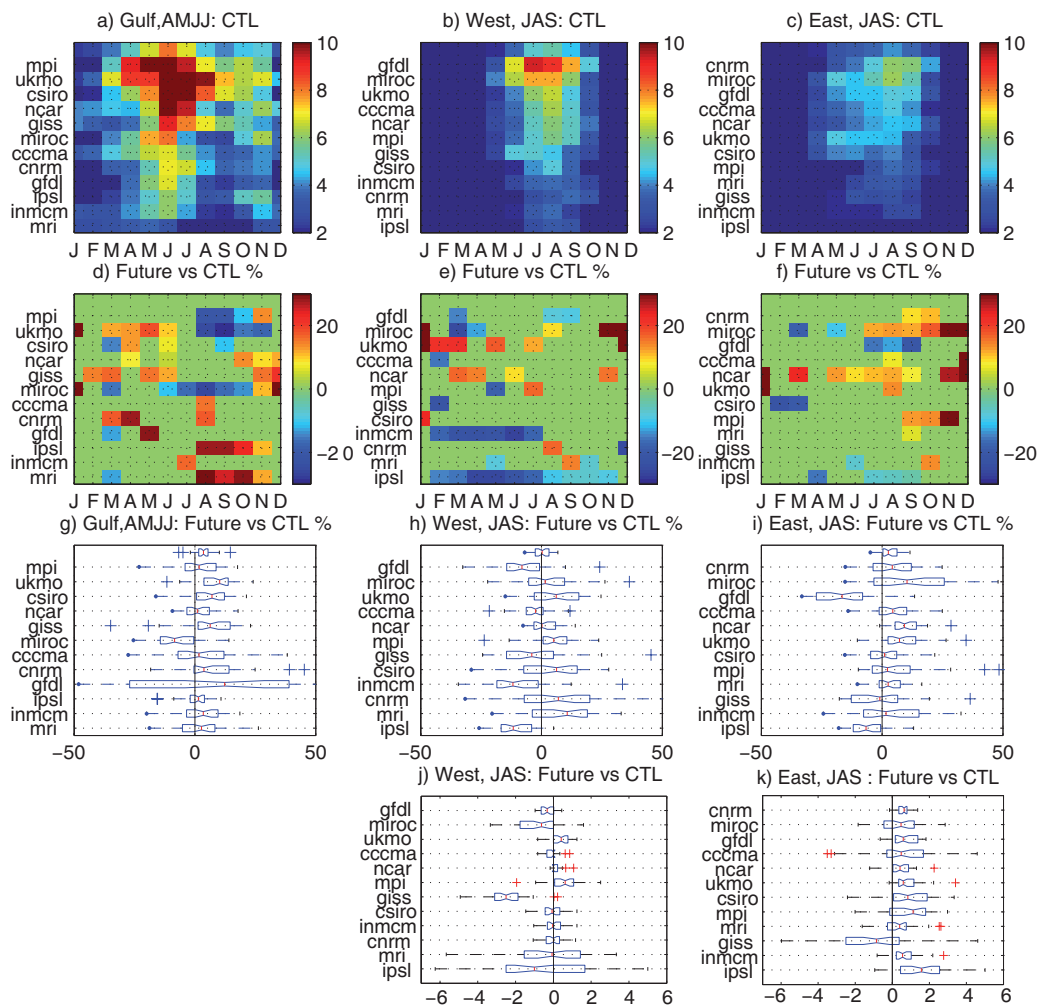


Figure 2: Simulated seasonal indexes averaged over key-regions,

(a,b,c) mean annual rainfall evolutions over the Gulf of Guinea [Eq-5N; 20W-10E] from April to June (1st column) and over the Western [5N-20N; 20W-0E] and Eastern [5N-20N; 0E-30E] continental parts of West Africa (columns 2-3). Model acronyms (y-axis) are sorted in descending order regarding individual seasonal amounts with the mean model ensemble at top

(d,e,f) significant ($p= 0.05$) precipitation change expressed in percents between years 1960-1999 and 2031-2070.

(g,h,i) notched-box plot as robust estimate of the uncertainty about the medians for box to box comparison. Each box has lines at the lower quartile, median, and upper quartile values, all expressed in percentages of precipitation change. Lines extending from each end of the box show the extent of the rest of the data between -50% and + 50%.

(j,k) as (g,h,i) but for the latitudinal location in degree of the centroid of the moisture flux convergence at 850 hPa averaged over a western (15°W -5°W; 0°-14°N) and a central-eastern (5°W- 20°E; 0°N-20°N) African regions. Here only 11 models out of 12 are considered since no moisture data were available in UKMO.

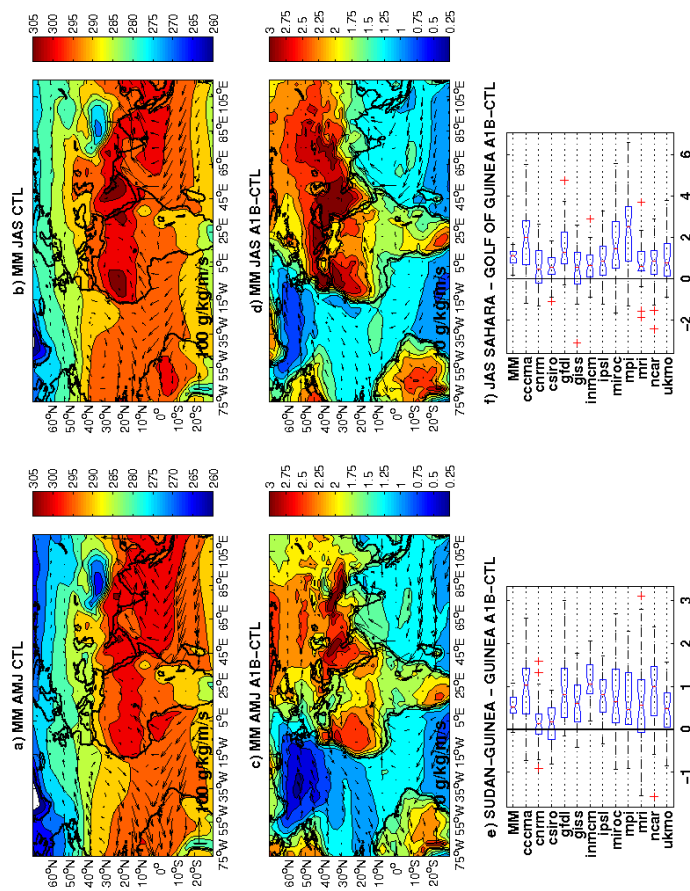


Figure 3. Simulated changes in air temperature near the surface, in moisture flux at 925 hPa (maps), and in air temperature gradients (boxplots) in AMJ (left) and JAS (right) (a,d): temperature in tenth of °C and moisture fluxes in g/kg/m/s from the ensemble mean (1960-1999) (b,e): differences in air temperature at 2m and in moisture fluxes at 925 hPa between years 1960-1999 and 2031-2070 (c,f): notched-box plot (as in fig. 2g-i), but for changes (in °C) in meridional air temperature gradient at 2m between 10°W and 0° longitude. In April-June (AMJ) the gradient refers to the difference between values averaged over [7.5°N-12.5°N] and over [5°S-Eq] while in July-September (JAS) the gradient is the difference between [20°N-15°N] and [5°S-Eq].